RSC Advances

PAPER

View Article Online
View Journal | View Issue

Cite this: *RSC Adv.*, 2021, **11**, 38202

Enhanced antibacterial activity of acid treated MgO nanoparticles on *Escherichia coli*†

Xiaoyi Li, Xiaoyu Hong, Yan Yang, * Jiao Zhao, * Catherine Sekyerebea Diko and Yimin Zhu*

Received 17th August 2021
Accepted 23rd November 2021

DOI: 10.1039/d1ra06221b

rsc.li/rsc-advances

Acid treatment is one of the effective methods that directly modifies surface physical and chemical properties of inorganic materials, which improves the materials' application potential. In this work, the surface modified MgO nanoparticles (NPs) were prepared through a facile acid-treatment method at room temperature. Compared with the untreated sample, the surviving *Escherichia coli* (*E. coli*, ATCC 25922) colonies of the modified MgO NPs decreased from 120 to 54 (10^2 CFU mL^{-1}). The enhanced antibacterial activity may be due to the improvement of oxygen vacancies and absorbed oxygen (O_A) content (from 41.6% to 63.1%) as confirmed by electron spin resonance (ESR) and X-ray photoelectron spectroscopy (XPS). These findings revealed that the acid treatment method could directly modify the surface of MgO NPs to expose more oxygen vacancies, which would promote reactive oxygen species (ROS) generation. The membrane tube and single ROS scavenging results further indicated that the increased antibacterial ability originated from the synergetic effect of ROS damage (especially $^{\bullet}O_2^-$) and direct contact between H-MgO NPs and *E. coli*.

1. Introduction

In recent years, microbial malignant proliferation and transmission, such as of *Enterohemorrhagic Escherichia coli*, *Candida Auris* and Corona Virus (COVID-19) are the major factors influencing the worldwide pandemic incidences, endangering environmental hygiene and human health.[1–3] Therefore, developing effective antibacterial nanomaterials that can destroy harmful microbes has become an urgent task. Compared with natural and organic antibacterial agents, inorganic nanomaterials have better heat stability and durability. Ag-type and photocatalytic antibacterial systems have shown potential in restraining bacterial growth and disease prevention. However, the application of Ag-type materials has been restricted due to their toxicity to human beings and high cost,[4] while the antibacterial activities of photocatalytic metal oxides (such as ZnO, TiO_2 and CdO) strongly depend on the wavelength and intensity of light.[5–7] Therefore, among different inorganic antibacterial agents, MgO NPs have attracted considerable attention because of their low cost, high stability and no need of illumination.[8] Thus, MgO NPs have been considered as the promising candidates for inorganic antibacterial agents. However, currently the antibacterial ability of MgO NPs is insufficient compared with Ag, TiO_2 and ZnO, which has limited their large-scale applications.[9–12]

To solve the above problem, researchers have used various strategies to enhance the antibacterial properties of MgO NPs. For example, through high temperature solution combustion technology,[8] hydrothermal method,[13] controlling calcination temperature[14] and elements doping (Li, Zn, Ti, Fe, Co, Ag, and Ni *etc.*) strategy.[15–20] In addition, using the co-doping, sol–gol and synthesis of composites with heterojunction structure methods could improve the antibacterial property of metal oxides.[21–23] Through the reformation of MgO NPs, many of these reports relate their high antibacterial activity of MgO NPs to the increase of oxygen vacancies. However, only the exposed oxygen vacancies (on the surface of MgO NPs) could work efficiently. Therefore, it is very challenging to find a suitable solution to directly modify the surface of MgO NPs to greatly enrich their surface oxygen vacancies and enhance their antibacterial activities.

Acid treatment is a facile and effective method that could modify the surface properties of materials (ZnO,[24] TiO_2,[25] In_2S_3,[26] MnO_2,[27] *etc.*). However, improving the antibacterial property of MgO nanomaterials by acid treatment is rarely reported. Herein, we presented a simple acid treatment method that could directly modify the surface of MgO NPs. The modified MgO NPs showed significantly increased antibacterial activity on *E. coli*, which might have originated from the abundant surface oxygen vacancies and increased O_A contents (from 41.6% to 63.1%), as confirmed by ESR and XPS results.

Dalian Maritime University, China. E-mail: yyang@dlmu.edu.cn; zhaojiao@dlmu.edu.cn; ntp@dlmu.edu.cn

† Electronic supplementary information (ESI) available. See DOI: 10.1039/d1ra06221b

The best acid treatment condition was in hydrochloric acid solution under pH = 2 for 1 h.

2. Experimental details

2.1 Materials

MgO was obtained from Tianjin Komeo Chemical Reagent Co., Ltd. (China). In the experiment, chemical reagents of analytical grade were purchased from Tianjin Guangfu Fine Chemical Research Institute (China) and used without further purification. All biological reagents were purchased from Beijing Aoboxing Biotechnology Co., Ltd. (China).

2.2 Acid treatment

The acid treated MgO NPs were prepared by a simple acid-treatment method. Firstly, the MgO NPs were processed by a high-energy ball milling method with a rotation speed of 500 rpm for 30 min. Secondly, 2.25 g of MgO NPs were impregnated in 30 mL of different acidic solutions (sulphuric acid, formic acid and hydrochloric acid) at pH = 2 for 1 h respectively at room temperature. After impregnation, the white powders were separated by centrifugation at 9000 rpm for 5 min and washed with deionized water for few times. Lastly, the obtained MgO NPs were dried in the oven at 110 °C for 12 h. When impregnated in hydrochloric acid solution, MgO NPs treated with different pH (pH = 2, 3 and 4) for 1 h and treatment time (0.5 h and 1 h) at pH = 2 were also obtained. The MgO NPs after high-energy ball milling was named as pure-MgO. Pure-MgO treated with hydrochloric acid (pH = 2) for 1 h was denoted as H-MgO.

2.3 Antibacterial activity test

The antibacterial activity of the acid treated MgO NPs was studied by the plate count method.[28] Briefly, the activated *E. coli* (ATCC 25922) was centrifuged at 6000 rpm for 5 min and washed with phosphate buffer saline (PBS) solution three times to obtain the *E. coli* suspension. The 10^8 CFU mL^{-1} of *E. coli* and 750 μg mL^{-1} of MgO NPs were added into the sterilized flask and then incubated at 37 °C in the shaking incubator (150 rpm). After 4 h, 100 μL of the diluted suspension was spread on solid agar plates. These plates were incubated at 37 °C for 24 h and the number of surviving *E. coli* colonies were counted.

2.4 Characterization

The crystal structure of the samples was observed by the X-ray diffractometer (XRD) with Cu Kα (λ = 1.5406 Å) radiation over the 2θ range of 10°–90° (PANalytical B.V., X'Pert Pro diffractometer, America). The surface morphology was recorded using a scanning electron microscope (SEM) with an accelerating voltage of 10 kV (ZEISS MERLIN Compact, Germany). High-resolution transmission electron microscopy (HR-TEM) was conducted on a JEM-2100F transmission electron microscopy (Japan) with an accelerating voltage of 200 kV to confirm the crystal lattice of samples. XPS analysis was carried out by an X-ray photoelectron spectrometer (ESCALAB 250, Thermo VG, America), and the spectra were calibrated referring to the C 1s peak (284.6 eV). The ESR spectra were detected on the instrument (JES-FA 300, JEOL, Japan) at room temperature. Fourier transform infrared (FTIR) spectra were recorded with an EQUINOX55 instrument (Bruker, Germany) in the transmittance mode.

2.5 Membrane tube test

The concentration of activated *E. coli* suspension was adjusted to 10^5 CFU mL^{-1} by diluting it with PBS solution. The samples were put into a membrane tube (Spectrum MD 10, America) with a molecular weight of 12 000–14 000. The membrane tube with MgO samples (300 μg mL^{-1}) was put into *E. coli* suspension. As a control, equal amounts of samples without membrane tube were added to *E. coli* suspension. After 24 h, the antibacterial ratio of the samples was calculated by the plate count method.

2.6 Single ROS scavenging test

The activated *E. coli* suspension (10^5 CFU mL^{-1}) and MgO samples (100 μg mL^{-1}) were mixed to prepare the suspension (named as suspension A). The superoxide dismutase (SOD, 100 unit per mL, 100 μL), catalase (CAT, 100 unit per mL, 100 μL) and D-mannitol (10 mM, 100 μL) were separately added into the suspension A and incubated in a shaking incubator (150 rpm) maintained at 37 °C for 20 min. The suspension A was not treated with any ROS scavenging agent as the control group. The antibacterial activity was evaluated by the plate count method.

3. Results and discussion

To compare the antibacterial performance of MgO NPs treated with different acidic solutions (sulphuric acid, formic acid and hydrochloric acid), the plate count method was used against *E. coli*. As shown in Fig. 1, in comparison to pure-MgO, a significant decrease was found in the survived bacteria colonies of acid treated MgO NPs, suggesting that acid treatment was effective for the enhancement of antibacterial activity. The representative photographs of the survived *E. coli* colonies are shown in Fig. S1 (ESI†). Amongst them, hydrochloric acid was the most efficient acid, with the survived bacteria colonies decreasing from 120 to 54 (10^2 CFU mL^{-1}) and this was relatively low compared with pure-MgO. Meanwhile, the antibacterial efficiency of pure-MgO was lower than ZnO and higher than TiO_2 as shown in Fig. S2 (ESI†). The low activity of TiO_2 might be attributed to the lack of UV or visible illumination.

To further determine the impact of hydrochloric acid treatment conditions on the MgO NPs' antibacterial performance, different pH (pH = 2, 3 and 4) for 1 h and treatment time (0.5 h and 1 h) at pH = 2 were evaluated in our work, as shown in Fig. 2. These results suggested that the appropriate acid concentration and treatment time were favorable for improving the antibacterial property of MgO NPs. The antibacterial activities were in the order of pH = 2 > pH = 3 > pH = 4. At pH = 2, from 0.5 h to 1 h, the antibacterial activity of MgO NPs increased with treatment time, with the surviving *E. coli* colonies decreased from 85 to 54 (10^2 CFU mL^{-1}). The photographs of

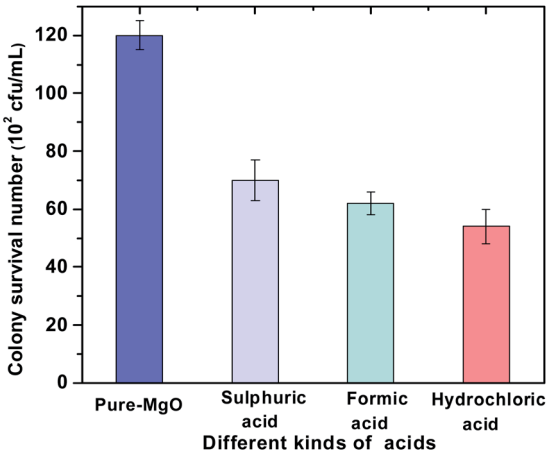

Fig. 1 The surviving bacteria colonies of MgO NPs treated with different acidic solutions (pH = 2) for 1 h.

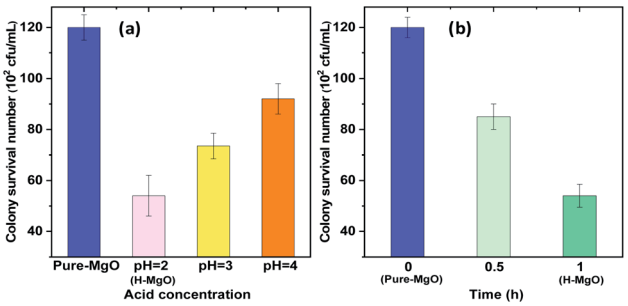

Fig. 2 The antibacterial activity of MgO NPs treated with hydrochloric acid at different pH for 1 h (a) and treatment time at pH = 2 (b).

the surviving *E. coli* colonies are also displayed in Fig. S3 and S4 (ESI†). These results indicated that the best acid treatment condition was in hydrochloric acid solution at pH = 2 for 1 h. Moreover, the acid treatment method was very convenient and could directly modify the MgO NPs surface, which might have resulted in their high performance.

To investigate the differences of MgO NPs before and after acid treatment, the crystalline phase, surface morphology, and microstructure were studied by XRD, SEM and HR-TEM, respectively. The XRD patterns of pure-MgO and H-MgO NPs are shown in Fig. 3. The diffraction peaks were observed at 36.9°, 42.9°, 62.3°, 74.7° and 78.6°, corresponding to the crystal planes (111), (200), (220), (311) and (222) of cubic MgO (JCPDS no. 45-0946), respectively. The characteristic peak at (200) of H-MgO moved to a lower angle, while the FWHM increased slightly in comparison with pure-MgO. Based on Scherrer's equation, the crystallite size of MgO NPs after acid treatment was decreased from 45.9 to 39.1 nm as shown in Table S1 (ESI†), which might be due to the acid etching on MgO NPs surface. In addition, the weak diffraction peaks of H-MgO at 18.5°, 37.9° and 58.6° were indexed to the (001), (101) and (110) crystal planes of $Mg(OH)_2$ phase (JCPDS no. 44-1482), indicating that a small amount of $Mg(OH)_2$ was formed during acid treatment. It is well known that MgO NPs will easily hydrated into $Mg(OH)_2$ in water (as shown in Fig. S5†).[29] According to the FTIR spectra in Fig. S6 (ESI†), the absorption bands positioned at 439 and 1419 cm^{-1} were associated with the vibrations of Mg–O and carbonate ions, and the peaks at 1627 and 3442 cm^{-1} were due to the bending and stretching vibrations of surface hydroxyl, respectively.[30] The sharp absorption peak appeared at 3705 cm^{-1} in H-MgO was attributed to the O–H stretching vibration generated by $Mg(OH)_2$, suggesting the existence of $Mg(OH)_2$ after acid treatment, which was consistent with the XRD results.[31] Interestingly, the antibacterial activity $Mg(OH)_2$ was much lower than that of pure-MgO and H-MgO as shown in Fig. S7 (ESI†). These results implied that the enhanced antibacterial efficiency was originated from acid treated MgO NPs.

The SEM analysis showed the surface morphologies of pure-MgO and H-MgO (Fig. 4a and b). Compared with pure-MgO, the surface of H-MgO became rough and the edges were sharper, owing to the presence of $Mg(OH)_2$, which agreed well with the XRD results. These results suggested that the acidic modification process could greatly increase the surface roughness of MgO NPs. To further investigate the surface microstructures,

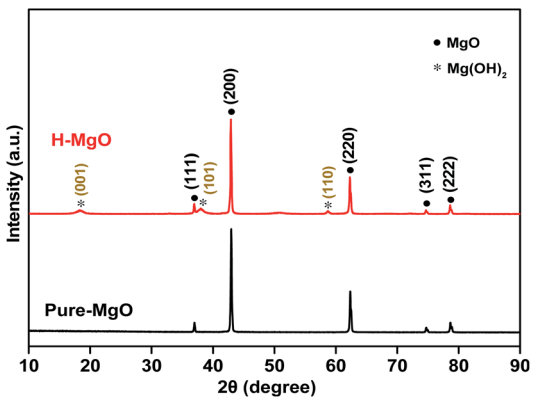

Fig. 3 XRD patterns of pure-MgO and H-MgO.

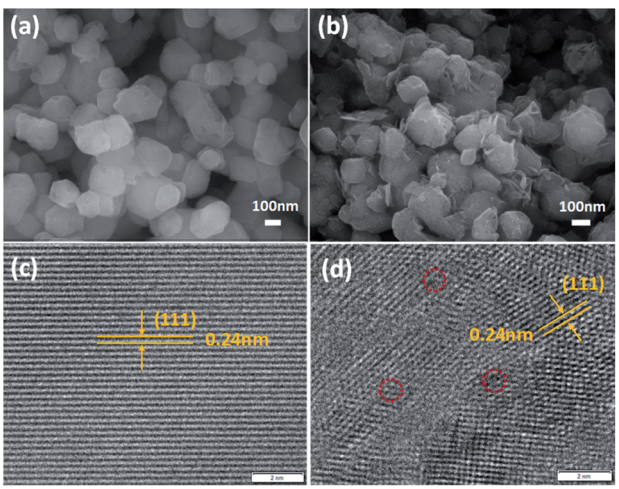

Fig. 4 SEM and HR-TEM images of pure-MgO (a and c) and H-MgO (b and d).

the HR-TEM images were recorded. Fig. 4c and d showed typical MgO patterns consistent with the (111) plane with the crystalline interplanar spacing of 0.24 nm.[13] These interplanar corresponded well with the *d*-spacing value of cubic MgO in the XRD results. Interestingly, pure-MgO had a highly ordered crystal lattice, while part of the microstructure of H-MgO was twisted. Moreover, the H-MgO showed more defects (as illustrated by the red circles in Fig. 4d) than pure-MgO, which might be caused by the acid treatment.[32]

To identify oxygen vacancies, the ESR measurement was adopted. The ESR signal was obtained from equal mass of MgO samples, thus the sample with stronger signal corresponds with more oxygen vacancies.[33] Compared with the pure-MgO, the signal intensity of H-MgO was significantly enhanced (Fig. 5), explicitly indicating that the concentration of oxygen vacancies was obviously increased after acid treatment, further supported the above hypothesis based on the HR-TEM results. Compared with the smooth surface microstructure of pure-MgO, the HR-TEM results revealed that regular crystal lattice of H-MgO became partly distorted. Meanwhile, the XRD results indicated the reduction of crystalline grains sizes from 45.9 to 39.1 nm after acid treatment, which might be caused by the acid-etching effect. When the MgO NPs surface were exposed to acidic solution, the deformation of surface lattice was easy to occur, and this process was accompanied by the formation of oxygen vacancies. These results were in line with previous studies.[34,35] In addition, it is well known that the strong chemisorption effect of oxygen vacancies to oxygen in air can increase the quantity of surface adsorbed oxygen.[15,34] To study the influence of acid treatment on the surface adsorbed oxygen of MgO NPs, XPS measurement was also utilized. As shown in Fig. 6a, the XPS signals of Mg and O were detected respectively. Moreover, the H-MgO showed much higher intensity of O 1s peaks than that of pure-MgO. To further characterize the oxygen differences between pure-MgO and H-MgO, high resolution XPS of O 1s spectra were employed. As illustrated in Fig. 6b and c, the low binding energy peaks at 529.3–530.6 eV and the high binding energy peaks of 531.0–531.5 eV were observed in each sample, relating to lattice oxygen (O_L) and absorbed oxygen (O_A), respectively.[17,36] Besides, the H-MgO exhibited a weak peak located at 533.0 eV, attributing to the hydroxyl oxygen of $Mg(OH)_2$, which was in good agreement with the XRD, SEM results and previous reports.[37] The O_A contents for pure-MgO and H-MgO were 41.6% and 63.1% respectively. Based on the above results, the increased O_A content in H-MgO mainly originated from the increased surface oxygen vacancies.

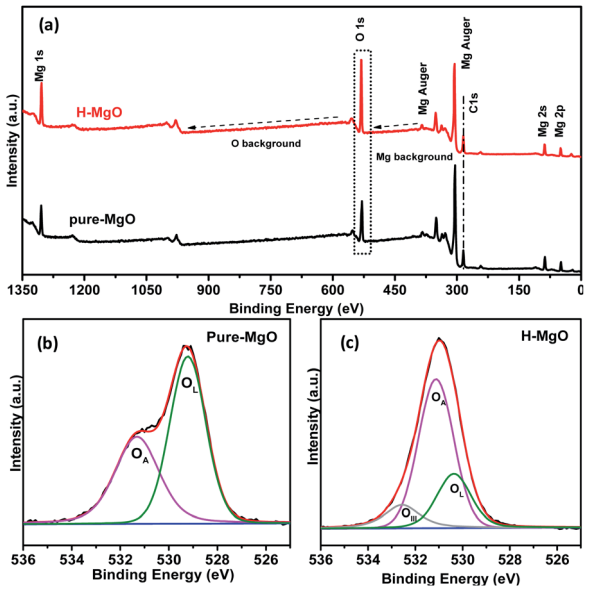

Fig. 6 XPS survey spectra of pure-MgO and H-MgO (a), O 1s XPS fine spectra of pure-MgO (b) and H-MgO (c).

At present, the antibacterial mechanism of MgO primarily includes ROS damage and MgO/*E. coli* contact.[38] To compare these two mechanisms, the antibacterial ratio of H-MgO was determined by using the membrane tube method. ROS and dissolved ions inside the tube could diffuse out to the *E. coli* solution, while H-MgO nanoparticles were limited within the

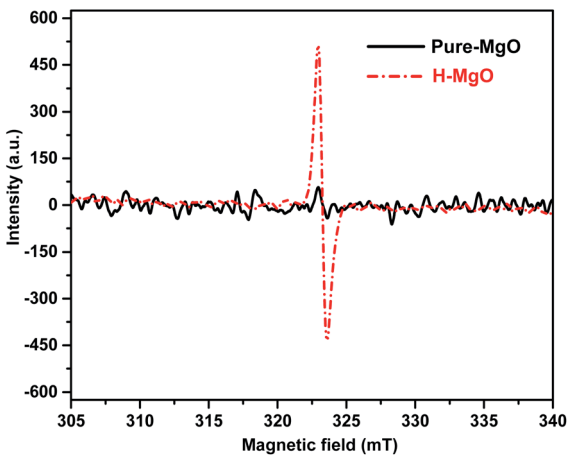

Fig. 5 ESR spectra of pure-MgO and H-MgO at room temperature.

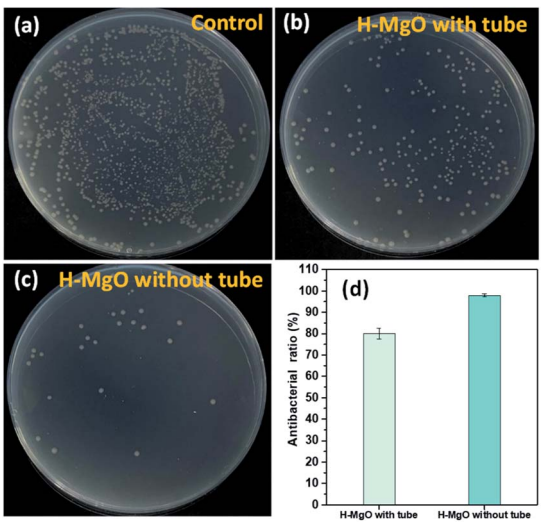

Fig. 7 The antibacterial activity of vontrol (a), H-MgO with tube (b), H-MgO without tube (c) and the antibacterial ratio (d).

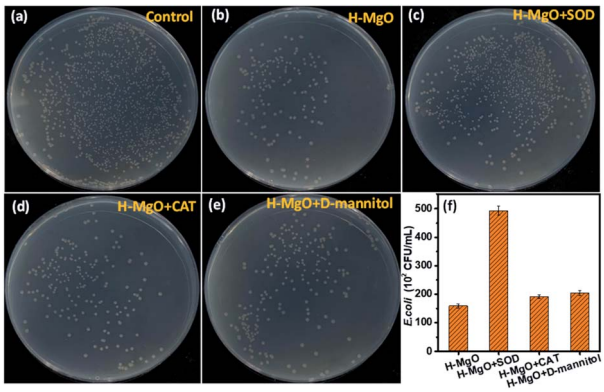

Fig. 8 The influence of single ROS scavenging agent on the antibacterial property of H-MgO.

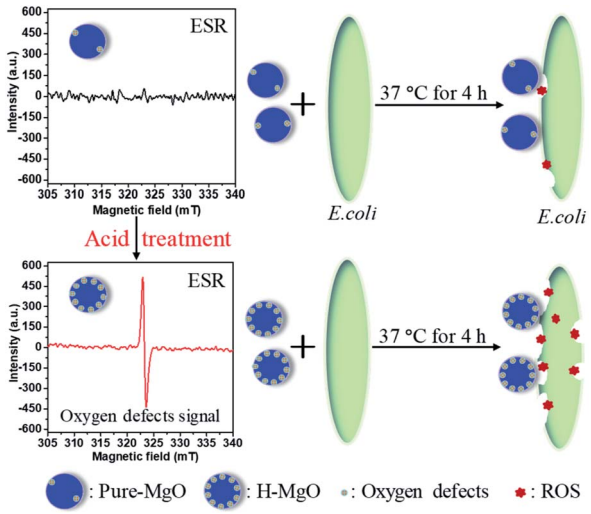

Fig. 9 Schematic of the antibacterial mechanism of H-MgO.

membrane tube preventing MgO/*E. coli* contact. As shown in Fig. 7, when H-MgO was limited within the membrane tube, the antibacterial ratio was ~80% while the contrast sample without membrane tube was 98%. The results proved that ROS might play key a role in the antibacterial mechanism, whereas MgO/*E. coli* contact played a supplementary role.

Based on the above results, ROS (including $^{\bullet}O_2^-$, $^{\bullet}OH$ and H_2O_2) and dissolved ions that directly leak out from the membrane tube has played the key role. Studies have indicated that releasing of dissolved Mg^{2+} in *E. coli* suspension has no effect on the antibacterial property of MgO.[38] Therefore, ROS is the main reason that caused the antibacterial property. Furthermore, to clarify which specie is the most effective, ROS scavenging tests were performed. Reagents like superoxide dismutase, catalase and D-mannitol can participate in the scavenging of $^{\bullet}O_2^-$, $^{\bullet}OH$ and H_2O_2, but on their own does not have antibacterial activity.[39] As shown in Fig. 8, compared to the surviving *E. coli* colonies of H-MgO without any ROS scavenging treatment [159 (10^2 CFU mL^{-1})], the colonies were increased to 493, 191 and 204 (10^2 CFU mL^{-1}) by adding SOD, CAT and D-mannitol respectively. These results suggested that $^{\bullet}O_2^-$ is the crucial factor in ROS damage in comparison with $^{\bullet}OH$ and H_2O_2.

From these results, the possible antibacterial mechanism of H-MgO was illustrated, as shown in Fig. 9. The acidic surface modification could create more oxygen vacancies on the H-MgO surface, which led to more adsorbed oxygen. These are conducive to producing more ROS (especially $^{\bullet}O_2^-$) and promoting the antibacterial ability.[34,40,41] Meanwhile, the contact damage was found helpful in the enhancement of antibacterial performance. Thus, the antibacterial mechanism of H-MgO was the synergetic effect of ROS damage and direct contact between MgO and *E. coli*.

4. Conclusion

In summary, a novel surface modification of MgO NPs was realized by a feasible acid treatment process. Compared with the untreated sample, the acid modified MgO NPs exhibited excellent antibacterial activity against *E. coli*, with the surviving bacteria colonies decreasing from 120 to 54 (10^2 CFU mL^{-1}). As confirmed by ESR and XPS, the oxygen vacancies and O_A content (from 41.6% to 63.1%) increased significantly after acid treatment, which was beneficial for the production of ROS and the enhancement of antibacterial efficiency. The membrane tube and single ROS scavenging results further confirmed that ROS especially $^{\bullet}O_2^-$ played a significant role in the antibacterial mechanism of H-MgO, while the direct contact effect played a partial role. Based on the synergism of ROS and direct contact between H-MgO NPs and *E. coli*, the acid treatment strategy was highly effective to enhance the antibacterial efficiency of MgO NPs. We believe this strategy could be suitable for other inorganic materials as well, which may shed light to the surface modification of inorganic materials.

Conflicts of interest

There are no conflicts to declare.

Acknowledgements

This work was financially supported by Liaoning Revitalization Talents Program (XLYC1907137) and Fundamental Research Funds for the Central Universities (3132019334).

References

1 C. Gadishaw-Lue, A. Banaag, S. Birstonas, A. S. Francis and D. B. Foster, *Infect. Immun.*, 2021, **89**, DOI: 10.1128/iai.00719-20.
2 C. W. Ong, S. C. A. Chen, J. E. Clark, C. L. Halliday, S. E. Kidd and D. J. Marriott, *Int. Med. J.*, 2019, **49**, 1229–1243.
3 S. Khavandi, E. Tabibzadeh, M. Naderan and S. Shoar, *Cont. Lens Anterior Eye*, 2020, **43**, 211–212.
4 M. Huang, A. A. Keller, X. M. Wang, L. Y. Tian, B. Wu, R. Ji and L. J. Zhao, *Environ. Sci. Technol.*, 2020, **54**, 15996–16005.

5 X. L. Xu, D. Chen, Z. G. Yi, M. Jiang, L. Wang, Z. W. Zhou, X. M. Fan, Y. Wang and D. Hui, *Langmuir*, 2013, **29**, 5573–5580.
6 J. Wang, L. Svoboda, Z. Nemeckova, M. Sgarzi, J. Henych, N. Licciardello and G. Cuniberti, *RSC Adv.*, 2021, **11**, 13980–13991.
7 A. Rahman, M. Aadil, S. Zulfiqar, I. A. Alsafari, M. Shahid, P. O. Agboola, M. F. Warsi and M. E. F. Abdel-Haliem, *Ceram. Int.*, 2021, **47**, 8082–8093.
8 Y. J. Hao, B. Liu, L. G. Tian, F. T. Li, J. Ren, S. J. Liu, Y. Liu, J. Zhao and X. J. Wang, *ACS Appl. Mater. Interfaces*, 2017, **9**, 12687–12693.
9 R. Dastjerdi and M. Montazer, *Colloids Surf., B*, 2010, **79**, 5–18.
10 H. M. C. De Azeredo, *Trends Food Sci. Technol.*, 2013, **30**, 56–69.
11 Y. H. Leung, A. M. C. Ng, X. Xu, Z. Shen, L. A. Gethings, M. T. Wong, C. M. N. Chan, M. Y. Guo and Y. H. Ng, *Small*, 2014, **10**, 1171–1183.
12 F. Luo, J. Lu, W. Wang, F. Tan and X. Qiao, *Micro Nano Lett.*, 2013, **8**, 479–482.
13 D. V. Ponnuvelu, A. Selvaraj, S. P. Suriyaraj, R. Selvakumar and B. Pulithadathail, *Mater. Res. Express*, 2016, **3**, 105005.
14 X. Li, J. Zhao, X. Hong, Y. Yang, X. Tang, Y. Zhu and T. Li, *ChemistrySelect*, 2020, **5**, 3201–3207.
15 K. Krishnamoorthy, G. Manivannan, S. J. Kim, K. Jeyasubramanian and M. Premanathan, *J. Nanopart. Res.*, 2012, **14**, 1063–1072.
16 Y. Rao, W. Wang, F. Tan, Y. Cai, J. Lu and X. Qiao, *Ceram. Int.*, 2014, **40**, 14397–14403.
17 Y. Rao, W. Wang, F. Tan, Y. Cai, J. Lu and X. Qiao, *Appl. Surf. Sci.*, 2013, **284**, 726–731.
18 X. Y. Hong, Y. Yang, X. Y. Li, M. Abitonze, C. S. Diko, J. Zhao, Q. Ma, W. F. Liu and Y. M. Zhu, *RSC Adv.*, 2021, **11**, 2892–2897.
19 T. Munawar, M. S. Nadeem, F. Mukhtar, A. Azhar, M. Hasan, K. Mahmood, A. Hussain, A. Ali, M. I. Arshad, M. A. Nabi and F. Iqbal, *Phys. B*, 2021, **602**, 412555.
20 T. Munawar, M. N. U. Rehman, M. S. Nadeem, F. Mukhtar, S. Manzoor, M. N. Ashiq and F. Iqbal, *J. Alloys Compd.*, 2021, **885**, 160885.
21 T. Munawar, M. S. Nadeem, M. N. U. Rehman, F. Mukhtar, M. Riaz and F. Iqbal, *J. Mater. Sci.: Mater. Electron.*, 2021, **32**, 14437–14455.
22 T. Munawar, F. Mukhtar, S. Yasmeen, M. Naveed-Ur-Rehman, M. S. Nadeem, M. Riaz, M. Mansoor and F. Iqbal, *Environ. Sci. Pollut. Res.*, 2021, **28**, 42243–42260.
23 T. Munawar, S. Yasmeen, M. Hasan, K. Mahmood, A. Hussain, A. Ali, M. I. Arshad and F. Iqbal, *Ceram. Int.*, 2020, **46**, 11101–11114.
24 H. Maki, T. Ikoma, I. Sakaguchi, N. Ohashi, H. Haneda, J. Tanaka and N. Ichinose, *Thin Solid Films*, 2002, **411**, 91–95.
25 D. Zhao, C. Chen, Y. Wang, H. Ji, W. Ma and L. Zang, *J. Phys. Chem. C*, 2008, **112**, 5993–6001.
26 Y. Gao, S. Zhang, X. Bu and Y. Tian, *Catal. Today*, 2019, **327**, 271–278.
27 Y. Jiang, G. Cheng, R. Yang, H. Liu, M. Sun, L. Yu and Z. Hao, *J. Solid State Chem.*, 2019, **272**, 173–181.
28 S. Yang, Y. Nie, B. Zhang, X. Tang and H. Mao, *Ceram. Int.*, 2020, **46**, 20932–20942.
29 N. Aničić, M. Vukomanović, T. Koklič and D. Suvorov, *Small*, 2018, **14**, 1800205.
30 K. Karthik, S. Dhanuskodi, C. Gobinath, S. Prabukumar and S. Sivaramakrishnan, *J. Photochem. Photobiol., B*, 2019, **190**, 8–20.
31 Y. J. Zheng, L. Y. Cao, G. X. Xing, Z. Q. Bai, J. F. Huang and Z. P. Zhang, *RSC Adv.*, 2019, **9**, 7338–7348.
32 Z. Su, W. Yang, C. Wang, S. Xiong, X. Cao, Y. Peng, W. Si, Y. Weng, M. Xue and J. Li, *Environ. Sci. Technol.*, 2020, **54**, 12684–12692.
33 X. L. Xu, D. Chen, Z. G. Yi, M. Jiang, L. Wang, Z. W. Zhou, X. M. Fan, Y. Wang and D. Hui, *Langmuir*, 2013, **29**, 5573–5580.
34 P. Zhou, Y. Y. Wang, C. Xie, C. Chen, H. W. Liu, R. Chen, J. Huo and S. Y. Wang, *Chem. Commun.*, 2017, **53**, 11778–11781.
35 Z. H. Li, H. T. Sun, Z. Q. Xie, Y. Y. Zhao and M. Lu, *Nanotechnology*, 2007, **18**, 165703.
36 K. Krishnamoorthy, J. Y. Moon, H. B. Hyun, S. K. Cho and S. J. Kim, *J. Mater. Chem.*, 2012, **22**, 24610–24617.
37 Y. C. Cai, C. L. Li, D. Wu, W. Wang, F. T. Tan, X. Y. Wang, P. K. Wong and X. L. Qiao, *Chem. Eng. J.*, 2017, **312**, 158–166.
38 Q. Z. Tian, J. W. Ye, W. J. Yuan, S. Q. Zhang, L. Shi, J. C. Zhong and G. L. Ning, *Powder Technol.*, 2020, **371**, 130–141.
39 S. Yang, Y. L. Nie, B. Zhang, X. N. Tang and H. M. Mao, *Ceram. Int.*, 2020, **46**, 20932–20942.
40 V. L. Prasanna and R. Vijayaraghavan, *Mater. Sci. Eng., C*, 2017, **77**, 1027–1034.
41 R. M. Diaz, P. E. Cardoso-Avila, J. A. P. Tavares, R. Patakfalvi, V. V. Cruz, H. P. L. de Guevara, O. G. Coronado, R. I. A. Garibay, Q. E. S. Arroyo, V. F. Marañón-Ruiz and J. C. Contreras, *Nanomaterials*, 2021, **11**, 410.